Seasonal dynamics of seawater CO_2 system at a coastal site near the southern tip of Izu Peninsula, Japan

Shigeki Wada[a,*], Masao Ishii[b], Naohiro Kosugi[b], Daisuke Sasano[b], Wakana Matsushita[c], Yuko Omori[d], Takeo Hama[d]

[a] *Shimoda Marine Research Center, University of Tsukuba, Shimoda, Shizuoka, 415-0025, Japan*

[b] *Oceanography and Geochemistry Research Department, Meteorological Research Institute, Japan Meteorological Agency, Tsukuba, Ibaraki, 305-0052, Japan*

[c] *Graduate School of Life and Environmental Sciences, University of Tsukuba, Tsukuba, Ibaraki, 305-8572, Japan*

[d] *Faculty of Life and Environmental Sciences, University of Tsukuba, Tsukuba, Ibaraki, 305-8572, Japan*

* *Corresponding author.*

E-mail address: swadasbm@shimoda.tsukuba.ac.jp (S. Wada)

tel: +81-558-22-6740; fax: +81-558-22-0346

ABSTRACT

To elucidate how variables of the seawater CO_2 system in surface waters have been changing seasonally and the mechanisms responsible for these changes in the area off the south coast of central Honshu Island, Japan, we made time-series measurements of total dissolved inorganic carbon (DIC), total alkalinity (TA), inorganic macronutrient and chlorophyll *a* concentrations as well as temperature and salinity at a near-shore station off Shimoda city near the southern tip of the Izu Peninsula over 19 months from November 2011 to June 2013. The oceanographic setting in our study site is characterized by seasonal stratification, low salinity in summer, and well-mixed water column in winter. A large bloom of phytoplankton developed in spring, thereafter nutrients were depleted within the mixed layer in summer. DIC exhibited large seasonal variations and ranged from 1967 μmol kg^{-1} in summer to 2073 μmol kg^{-1} in winter when normalized to a salinity of 35, because of biological production in the spring and summer and vertical mixing in autumn and winter, as shown by multiple regression analysis in which variations of normalized DIC (nDIC) are estimated from variations in temperature (13.3 to 25.5 °C) and chlorophyll concentrations (0.27-3.9 μg l^{-1}). We observed a decrease of TA due to dilution by precipitation and river runoff in summer and a trend of salinity-normalized TA increase over time. The saturation state of the calcium carbonate mineral aragonite Ω_{arg} varied seasonally from 2.40 in winter to 3.58 in summer. The Ω_{arg} in the present study was calculated using DIC, TA, temperature and salinity, and we applied sensitivity analysis for these parameters. Ω_{arg} was predominantly controlled by the large variations of DIC. The combination of these results from the station off Shimoda and from an offshore station at 34°N, 137°E to the west allow us to predict Ω_{arg} with high precision for temporal and spatial variations. It suggests that in winter, there is a meridional gradient of Ω_{arg} in the region off the

southern coast of central Honshu Island, with considerably lower Ω_{arg} in the coastal zone.

Keywords: CO_2 system, calcium carbonate saturation state, coastal zone, seasonal variability, south coast of central Honshu

1. Introduction

The partial pressure of carbon dioxide (pCO_2) in the atmosphere has been increasing over the past two centuries because of CO_2 emissions associated with human activities such as fossil fuel combustion and land-use change (Prentice et al. 2001). In 2015, pCO_2 exceeded 400 ppm, 44% higher than the concentration during the pre-industrial era (WMO 2016). The increase of atmospheric CO_2 is causing global warming because CO_2 is a greenhouse gas (IPCC 2013). The ocean has played an important role in mitigating the impact of the atmospheric CO_2 increase by absorbing approximately a quarter of the CO_2 that has been emitted by human activities (Le Quéré et al. 2014). However, absorption of CO_2 by the ocean is leading to another problem referred to as ocean acidification (Caldeira and Wickett 2003). The pH of surface seawater has decreased by 0.1 since the 18th century, an approximately 30% increase of hydrogen ion activity (Doney et al. 2009), and it is projected to decrease by another 0.3–0.4 by the end of the 21st century in the highest CO_2 emission scenarios (Ciais et al. 2013).

Dissolved inorganic carbon (DIC) in aqueous solution takes three chemical forms: dissolved CO_2 (and a small fraction of carbonic acid, H_2CO_3), bicarbonate ion (HCO_3^-), and carbonate ion (CO_3^{2-}). These chemical species constitute the CO_2 system and are in

equilibrium with each other. Bicarbonate ion is the dominant form of DIC (~90%) under the weakly basic conditions (pH = ~8) found in seawater. Carbonate ion and aqueous CO_2 account for only a small fraction of the DIC in seawater. Absorption of CO_2 by seawater perturbs the CO_2 system and causes increases of the hydrogen ion activity (decrease of pH) and concentration of aqueous CO_2, and a decrease of the carbonate ion concentration. One of the important consequences of these changes is that the calcium carbonate saturation state (Ω) decreases, and calcification by marine organisms is therefore diminished. This decrease of Ω endangers calcifying organisms such as corals, coralline algae, gastropods, mollusks, and echinoderms (Pörtner et al. 2004; Anthony et al. 2008; Fabry et al. 2008; Kroeker et al. 2013). It has also been suggested that the increase of hydrogen ion activity inhibits the growth of some phytoplankton groups such as the Haptophyte *Chrysochromulina* sp. (Hama et al. 2012) as well as that of crustaceans and fishes (Pörtner et al. 2004). In contrast, some organisms are likely to benefit from these changes. For example, seagrasses have been found to flourish in a benthic ecosystem in a high-CO_2 area around a shallow volcanic CO_2 seep in the Mediterranean Sea (Hall-Spencer et al. 2008). Increases of phytoplankton biomass have also been observed under simulated high-CO_2 conditions in a mesocosm experiment (Riebesell et al. 2007) and in coastal phytoplankton cultures under low-nutrient conditions (Hama et al. 2016; Eberlein et al. 2017). The activities of phytoplankton can be enhanced by increasing the concentration of aqueous CO_2 in seawater (Kroeker et al. 2013), but the concomitant acidification of the seawater gives rise to changes in physiological processes such as ion balancing (Pörtner et al. 2004; Rivest and Hofmann 2014) and can therefore perturb normal metabolic pathways in marine organisms (Pörtner et al. 2004; Michaelidis et al. 2007). Because of the various impacts that changes of the seawater CO_2 system can have on marine organisms, there has been growing concern in recent years that significant

98 changes in marine ecosystems may occur in the near future.

99 The seawater CO_2 system is affected not only by the exchange of CO_2 with the
100 atmosphere but also by the uptake and release of CO_2 associated with photosynthesis and
101 respiration (Hofmann et al. 2011), formation and dissolution of the carbonate shells of
102 marine calcareous organisms (Albright et al. 2013), and ocean circulation and mixing
103 (Dumousseaud et al. 2010). All of these processes may be perturbed in one way or another
104 by global warming and/or ocean acidification. Secular changes in the seawater CO_2
105 system due to the influx of anthropogenic CO_2 into the ocean are now superimposed on
106 the spatial and temporal fluctuations of this system as a result of a variety of naturally
107 occurring processes (Ishii et al. 2011). These natural fluctuations can either enhance or
108 suppress the impact of ocean acidification on marine organisms and ecosystems (McNeil
109 and Matear 2008; Cornwall et al. 2013; Britton et al. 2016). To project when and how
110 marine ecosystems will be impacted by the secular trend of ocean acidification, it is
111 therefore important to understand the nature of these fluctuations and their controlling
112 mechanisms as well as the response of marine organisms to changes in the CO_2 system.

113 The Kuroshio Current is a strong boundary current in the western North Pacific that
114 delineates the northwestern edge of the North Pacific subtropical gyre (Barkley 1970).
115 The composition of marine biota changes greatly from one side of the Kuroshio to the
116 other. The region to the south of Kuroshio—the subtropical gyre—is mostly oligotrophic.
117 In contrast, the narrow zone between the Kuroshio and the south coast of Honshu Island,
118 Japan, which we refer to as the Honshu South Coastal Zone (HSCZ) in this study, is
119 characterized by high productivity (>200 gC m^{-2} $year^{-1}$; Yokouchi et al., 2007) and a large
120 diatom biomass (80 to 270 mg m^{-2}) during the spring bloom (Sugisaki et al. 2010). This
121 zone is the spawning ground for many species of pelagic fish (Sassa et al. 2004). In
122 addition, the northern limit of the habitat of hermatypic corals in the North Pacific lies

within this zone (Veron and Minchin 1992). The implication is that the HSCZ may provide a refugium for tropical corals that are being threatened by ocean warming (Yamano et al. 2011). However, a numerical simulation with an atmospheric-ocean climate model has suggested that the poleward migration of tropical corals may be blocked by the progression of ocean acidification toward the equator (Yara et al. 2012).

The Japan Meteorological Agency (JMA) is monitoring the changes of the CO_2 system as well as other biogeochemical and physical properties in the HSCZ as a part of its operational repeat measurements along the 137°E meridian from 34°N in the HSCZ to 3°N in the tropics. From this repeat section, it has been found that the salinity-normalized (to $S = 35$) concentration of DIC in the surface layer of the HSCZ varies greatly among seasons (1970 μmol kg^{-1} in summer to 2090 μmol kg^{-1} in winter) and is out of phase with the large variations of temperature (14–27 °C) (Ishii et al. 2011). The large seasonal variability of the DIC concentration leads to a large seasonal range of the saturation state of the calcium carbonate mineral aragonite (Ω_{arg}: 2.4 in winter to 3.7 in summer) (Ishii et al. 2011). This scenario contrasts with a smaller seasonal variability in the northern subtropics within and to the south of the Kuroshio (1960–2000 μmol kg^{-1} for DIC, 19–29 °C for temperature and 3.2–3.8 for Ω_{arg}) (JMA 2019). The larger seasonal variability of DIC in the HSCZ reflects the shallow mixed layer in summer, the high concentrations of DIC and nutrients below the mixed layer, entrainment into the surface mixed layer in winter, and the large seasonal variability of biological production. However, there is a logistical problem with the monitoring of the HSCZ by the JMA because the sampling frequency has been approximately once every 3 months or less. This sampling frequency is insufficient to capture details of the seasonal biogeochemical dynamics associated with the changes in physical conditions and biological activities in the HSCZ. For example, surface stratification during the warming season and deepening of the mixed layer during

148 the cooling season occur on a timescale of one month (Ara et al. 2011), and the abundance
149 of marine phytoplankton can also fluctuate widely on even a shorter timescale in response
150 to variations of environmental conditions (Miyashita 2005).

151 In this study, we made time-series measurements of CO_2 system variables together
152 with other biogeochemical and physical parameters such as temperature and salinity as
153 well as concentrations of nutrients and chlorophyll at a near-shore station within the
154 HSCZ near the southern tip of the Izu Peninsula, about 250 km to the east of 137°E (Fig.
155 1). The measurements were repeated over 19 months from November 2011 to June 2013
156 at intervals of one week to one month. Although this observation period was too short to
157 determine secular trends of ocean acidification, the high-frequency measurements at this
158 site enabled us to investigate the seasonal dynamics and short-term trends of the seawater
159 CO_2 system and the mechanisms responsible for the temporal variations. Seasonal
160 variations in the saturation state of aragonite in the surface layer were expressed
161 diagnostically with temperature and Chl *a* concentration as independent variables. This
162 equation was then used to elucidate the spatial and temporal variability of the aragonite
163 saturation state within the HSCZ.

164 **2. Materials and methods**

165 The time series measurements were obtained at 34°38'5N, 138°56'58E, about 1 km
166 off the coast of Shimoda City near the southern tip of the Izu Peninsula and to the east of
167 the Suruga Trough (Fig. 1). In the present study, we defined this site as “near-shore site”.
168 The water column at this site is 48 m deep, and the station is located on the upper slope
169 of an ocean trough. We carried out measurements and samplings at time intervals of
170 nominally one-half to one month from 28 November 2011 to 25 June 2013 from the
171 research vessel *Tsukuba* of the Shimoda Marine Research Center, University of Tsukuba.

The seawater samples were collected regularly at approximately 9:00 a.m. local time at depths of 1, 10, 20, and 30 m using 10-L Niskin bottles that had been pre-washed with 0.5 N hydrochloric acid.

Subsamples for DIC and total alkalinity (TA) analyses were introduced into 250 cm^3 borosilicate glass bottles (Schott Duran®) through polyethylene tubes and fixed with 200 μl of a saturated $HgCl_2$ solution according to the procedures described by Dickson et al. (2007) and Saito et al. (2008). The stopper of each glass bottle was lubricated with Apiezon L grease to prevent gas exchange with the atmosphere. Other sub-samples were filtered through a precombusted glass fiber filter (GF/F, Whatman), and the filters were stored at −80 °C. The filtrates were transferred into acid-cleaned polycarbonate bottles and stored at −20 °C prior to nutrient analysis. Conductivity, temperature (*t*), depth, and chlorophyll fluorescence were measured throughout the water column from the surface to a depth of 40 m with a conductivity-temperature-depth (CTD) sensor equipped with a chlorophyll fluorescence sensor (Idronut, Ocean Seven).

The chlorophyll *a* concentration (Chl *a*) was also measured for discrete samples by high-performance liquid chromatography (HPLC). The filter was immersed in *N*,*N*-dimethyl formamide (DMF) containing canthaxanthin as an internal standard, and the Chl *a* was extracted by sonication. The extracts were filtered through a polytetrafluorethylene (PTFE) filter with a 0.45-μm pore size and injected into an HPLC system (Agilent, 1100 series) with an Eclipse XDB-C8 liquid chromatography column (Agilent) after addition of tetrabutyl ammonium acetate (TBAA, 28 mM) and DMF. The procedure is described in more detail by Hama et al. (2016). Fluorescence, which was monitored with a chlorophyll sensor attached to the CTD, was found to be strongly correlated with the Chl *a* concentration measured by HPLC for discrete samples ($r^2 = 0.923$, $n = 44$). We therefore converted the fluorescence intensities into Chl *a* concentrations using a linear regression.

197 Vertical distributions of Chl *a* were fitted with a Gaussian function by a least squares
198 method, as described by Gong et al. (2015).

199 The concentrations of inorganic nutrients (nitrate+nitrite, ammonium, and phosphate)
200 were determined with an AutoAnalyzer (AACSII, BRAN+LUEBBE) (Hansen and
201 Koroleff 2007). The detection limits for nitrate+nitrite, ammonium, and phosphate were
202 0.050, 0.29, and 0.09 μM, respectively.

203 Concentrations of DIC were measured using an automated DIC analyzing unit
204 equipped with a CO_2 extraction unit and a coulometer (Nippon ANS, Inc., Japan). TA was
205 measured using an automated TA analyzing unit (Nippon ANS, Inc., Japan) based on
206 open-cell titration and a single-point titration using bromocresol green as an indicator dye
207 (Yao and Byrne 1998). The pH after the titration was determined spectrophotometrically
208 by CCD spectrophotometer (Model C10083CA, Hamamatsu Photonics K.K., Japan).
209 Both units were calibrated using Certified Reference Materials (Batch 105 and 113)
210 provided by Dr. A. Dickson of the Scripps Institution of Oceanography. Accuracies of
211 measurements, which were determined by the difference between measured and certified
212 value, were ±3 μmol kg^{-1} for DIC and ±1 μmol kg^{-1} for TA. Precisions determined by the
213 measurements of replicate samples were ±2 μmol kg^{-1} for DIC and ±1 μmol kg^{-1} for TA.
214 The saturation states of aragonite (Ω_{arg}) and calcite (Ω_{cal})—expressed with Eq. (1) and Eq.
215 (2), respectively—were calculated from DIC, TA, temperature, and salinity using the
216 CO2SYS program (Pierrot et al. 2011) with the dissociation constants of carbonic acid
217 given by Lueker et al. (2000) and stoichiometric solubility products K_{sp}' for aragonite and
218 calcite given by Mucci (1983).

219 $$\Omega_{arg} = [Ca^{2+}][CO_3^{2-}] / K_{sp}'_{arg} \quad (1)$$

220 $$\Omega_{cal} = [Ca^{2+}][CO_3^{2-}] / K_{sp}'_{cal} \quad (2)$$

In the calculations, concentrations of phosphate and silicic acid were not considered. The error associated with this omission is considered to be small (~0.01) because the concentrations of phosphate and silicate were relatively low (less than 0.7 and 9.5 μM respectively). The effect of silicic acid on Ω is small (~0.01) even at concentrations as high as 20 μM.

Parameters of carbonate chemistry were modeled with multi linear regression with R version 3.5.2 (R Core Team 2018). As discussed later, potential alkalinity (pTA: total alkalinity plus NO_3+NO_2), normalized DIC (nDIC = DIC·35/S) and Ω_{arg} were expressed as shown in Table 1. The equation in the present study is applicable only to interpolation within the monitoring period (November 2011 to June 2013). The ratios of DIC versus NO_3+NO_2 and NO_3+NO_2 versus PO_4 were analyzed by Model II regression using R version 3.5.2 (R Core Team 2018), because DIC and nutrients are not independent variables.

For comparison with our results, we used the datasets collected at 34ºE,137ºN (offshore site on upper slope of ocean trough) from November 2011 to June 2013, which has been published by JMA (2019).

3. Results

3.1. Temperature and salinity

The seawater temperature exhibited a pronounced seasonal cycle, ranging from 13.3 to 25.5 °C at the sea surface (Fig. 2a). Mixed layer depth (MLD), which was defined to be the depth at which the temperature is 0.5 °C lower than the temperature at a depth of 1 m (Foltz 2003), was consistently shallow in spring–summer from May through September because of surface heating, but MLD was also shallow in January 2012 and

February 2013 (Fig. 2b). From July through September, the surface layer was also characterized by relatively low salinity ($S < 33.5$) (Fig. 2c). In contrast, the water column was characterized by relatively high salinity ($S > 34.0$) in the cold ($T < 17$ °C) and vertically well-mixed winter season.

3.2. Chlorophyll a

The maximum chlorophyll *a* concentrations appeared in the subsurface layers in Spring to Summer season (April to August 2012 and April to June 2013) mainly at depths of 10–15 m (Fig. 2d). The most distinct subsurface chlorophyll maximum with a peak concentration of 3.5 mg m^{-3} was observed in July 2012. From December through February, the Chl *a* concentration was consistently low (between 0.3 and 0.79 mg m^{-3}).

3.3. Nutrients

The NO_3+NO_2 and PO_4 concentrations also exhibited large seasonal variations. The maximum concentrations, 9.9 μM for NO_3+NO_2 and 0.76 μM for PO_4, were observed in January 2013 (Figs. 3a, b). Concentrations were also high (8.1 and 0.60 μM, respectively) in the surface layer in mid-February 2012. They decreased to 1.2 and 0.17 μM, respectively, by mid-April as the mixed layer warmed. From November 2011 to March 2012 and from October 2012 to March 2013, concentrations of NO_3+NO_2 and PO_4 again increased (from 1.8 to 8.4 μM and from 0.14 to 0.65 μM, respectively), and concentrations of both nutrients were almost vertically uniform. The NH_4 concentration dynamics were considerably different from those of NO_3+NO_2 and PO_4 (Fig. 3c), and there was no significant correlation between NH_4 concentrations and the concentrations of either NO_3+NO_2 or PO_4. NH_4 constituted a minor fraction (8.1 ± 8.9%) of dissolved inorganic nitrogen, but in nutrient depleted conditions such as in the surface layer in summer, the

contribution of regenerated production using NH_4 could be important (Bode et al. 2002). However, we were unable to determine the contribution of NH_4 in detail, as we did not measure NH_4 uptake rates.

3.4. Total alkalinity

TA ranged from 2237 to 2287 μmol kg^{-1} (Supplementary Fig. S1). The lowest value was recorded in the surface layer in August 2012, when salinity also reached its minimum. In general, TA closely tracked salinity (Schneider et al. 2007; Jiang et al. 2014). When TA was salinity-normalized at S = 35 to exclude the effects of freshwater, the salinity-normalized TA (nTA = TA· 35/S) varied from 2313 to 2371 μmol kg^{-1} (Fig. 4a).

3.5. Dissolved Inorganic Carbon

DIC also exhibited a large seasonal variation from 1927 μmol kg^{-1} in summer to 2068 μmol kg^{-1} in winter (Supplementary Fig. S2). To correct the DIC changes for effects due to dilution/concentration of seawater by precipitation/evaporation and thereby to reveal the variations caused by biological activity and mixing, we normalized the DIC values to S = 35 (nDIC) as defined.

During the time-series measurements, nDIC ranged from 2012 to 2122 μmol kg^{-1}, and the amplitudes of the seasonal variation were 110 μmol kg^{-1} at 1 m depth, 99 μmol kg^{-1} at 10 m, 94 μmol kg^{-1} at 20 m, and 93 μmol kg^{-1} at 30 m (Fig. 4b). In 2013, the highest nDIC (2121 μmol kg^{-1}) was observed in January, and in 2012, the highest nDIC (2117 μmol kg^{-1}) was observed in December. In the surface layer (at 1 m and 10 m), nDIC decreased to 2032 μmol kg^{-1} by early May, as surface waters warmed. In the stratified and warm season from May to early November 2012, nDIC remained relatively low (2012 to 2052 μmol kg^{-1}), but nDIC again increased rapidly to ~2117 μmol kg^{-1} throughout the

water column in mid-December, as the surface waters cooled. In the lower layers (at depths of 20 m and 30 m), the nDIC time series included two peaks each year (Fig. 4(b)). One peak occurred in winter as described above, and the other peak occurred in summer (2105 μmol kg^{-1} in July 2012).

In this study, we calculated Ω_{arg} from the DIC, TA, temperature, and salinity data, and we determined that Ω_{arg} ranged from 2.42 to 3.58 at the time-series station off Shimoda (Fig. 4c). In the surface layer, Ω_{arg} was higher in summer and became lower when the temperature declined and DIC concentrations increased. A similar pattern has been observed at 34°N, 137°E in the western HSCZ (Ishii et al. 2011), which we defined as an "offshore site".

Due to higher DIC, the minimum value of Ω_{arg} (2.42) observed at the near-shore site (Shimoda) in winter was lower than at the offshore site (34°N, 137°E), where the lowest value of Ω_{arg} was 2.58 (JMA 2019). At the near-shore site, temperature ranged from 13.3 to 25.5ºC, which is slightly lower than at the offshore site (15.3-26.4ºC). Since Ω_{arg} increases with increasing water temperature, we should consider difference of temperature between the sites. The differences of temperature between the near-shore and offshore sites are less than 0-5 ºC. Assuming an increase of surface temperature by 5ºC, Ω_{arg} increases by 0.069-0.12. This is smaller than the difference between the sites (0.16), showing the contribution of another factor such as DIC. Values of Ω_{arg} of less than 2.9 were also found at depths of 20 and 30 m in July as a result of the DIC increase.

4. Discussion

4.1. Comparison of hydrography, Chl a and nutrients with previous studies in the HSCZ

Seasonality of hydrography, Chl *a* and nutrients at our study site are similar to those at other sites in the HSCZ. For example, CTD monitoring has been carried out for 9 years

316 in Sagami Bay, which is located in the eastern HSCZ (Fig. 1), and seasonal warming in
317 Sagami Bay has been observed along with a decline of salinity in summer (Miyaguchi et
318 al. 2006; Ara et al. 2011). Shoaling of the MLD and decreases of salinity in summer have
319 also been observed in the surface layer at offshore site at 134°N, 34°E and in the Kumano
320 Sea in the western HSCZ (Ishii et al. 2011; Mie Prefectural Government 2014; JMA 2019).
321 Urakawa et al. (2015) have compiled a monthly dataset of climatological mean sea
322 surface salinity in the coastal region around Japan with a horizontal resolution of 0.1°
323 from observational data collected from 1961 to 2010 and stored at the Japan
324 Oceanographic Data Center. They have shown that the decrease of salinity in summer is
325 a common phenomenon that occurs in the surface layer of the HSCZ from July through
326 October.

327 The depth-integrated chlorophyll *a* (Chl_{int}), calculated by numerical integration from
328 the surface to a depth of 30 m, ranged from 8.4 to 90 mg m^{-2}. The values of Chl_{int} were
329 relatively higher in mid-April to early May in 2012 (30 mg m^{-2}) and in mid-April 2013
330 (90 mg m^{-2}), which were associated with spring phytoplankton blooms. Significant spring
331 blooms have also been observed in other sites in the HSCZ such as Sagami Bay and the
332 Kumano Sea (Miyaguchi et al. 2006; Baki et al. 2009; Omote and Hatanaka 2011; Ara et
333 al. 2011).

334 The dramatic decrease of nutrient concentrations during this time of the year appears
335 to have been associated with the spring phytoplankton bloom, which was evidenced by
336 an increase of Chl_{int}. The concentrations of these nutrients were very low in the surface
337 layer from early May through early November 2012, when the upper water column was
338 stratified by warming and freshening. Vertical mixing began to occur in autumn (Figs. 3a,
339 b), and there was concomitant deepening of the nutricline with time. Seasonal changes of
340 NO_3+NO_2 and PO_4 concentrations were significantly correlated ($r^2 = 0.971$, $n = 89$, $p <$

0.01), with a $\Delta N/\Delta P$ ratio of 14.0 ± 0.3, which is within the expected range (Martiny et al. 2013a). In HSCZ region, similar values of the molar N/P ratio had been reported (12.2-15.9; Kamatani et al. 1981, 2000; Kinoshita et al. 2002; Ara and Hiromi 2008).

4.2. Variations of carbonate chemistry

During short periods of time, variations of TA were probably controlled by

1) evaporation and precipitation that concentrate or dilute seawater without changing the nTA,
2) dilution with river runoff with a very low salinity but some TA,
3) vertical and horizontal mixing of waters that contain different levels of TA,
4) net uptake or release of NO_3+NO_2 associated with biological activity,
5) formation or dissolution of the calcium carbonate shells of calcareous organisms.

To investigate the importance of these factors, we plotted TA against salinity (Fig. 5a). It was apparent that the wintertime TA increased from 2273 ± 6 μmol kg^{-1} during December 2011 to March 2012 to 2288 ± 6 μmol kg^{-1} during December 2012 to March 2013. During that same time, salinity decreased from 34.26 ± 0.09 to 34.11 ± 0.08. These changes in TA and salinity were consistent with the changes of TA and salinity with depth that were observed at 34°N, 137°E (JMA 2019) (Fig. 5a). The implication is that at the study site there was an increase of mixing with deeper water from above the slope of the Suruga Trough or Sagami Trough during December 2012 to March 2013. By contrast, when salinity decreased during the summer, the TA also decreased. In most of the samples taken in summer, the decreases of TA and salinity were consistent with water from the preceding winter being diluted by precipitation in summer.

The values of nTA at our study site ranged from 2313 to 2371 μmol kg^{-1}. At the

surface layer in summer, there was small peak of nTA (Fig. 4a). The implication is that there was a contribution of river runoff to the TA and/or there was biological uptake of NO_3+NO_2. The fact that NO_3+NO_2 decreased by ~8 μmol kg^{-1} from winter 2012 to summer 2012 suggests its potential effect on TA increase in summer. We quantified the effect on TA of river runoff and the upward movement of deep water using the relationship between TA and salinity (*S*).

The term pTA represents the potential alkalinity, which is equal to TA+$[NO_3^-]$+$[NO_2^-]$ (Brewer and Goldman 1976). Potential alkalinity is conservative if there is net biological uptake or release of NO_3 and NO_2. The intercept in the multi-regression analysis of pTA implies the pTA of river runoff (pTA^{river}) that contributes to the dilution of seawater in summer. The estimated pTA^{river} of 506 ± 85 μmol kg^{-1} (Table 1) is consistent with the TA of 521–672 μmol kg^{-1} measured in the Kiso River and other major rivers (Taguchi et al. 2009) that flow into Ise Bay and potentially influence the HSCZ. This result indicates that the decrease of salinity in summer in the upper water column at the study site was attributable to the dilution of seawater by river runoff. If TA^{river} = 506 μmol kg^{-1} and the salinity of seawater is diluted with river runoff from 34.2 to 33.3 in summer, the TA decrease in the surface layer is 14 μmol kg^{-1} less than if the river water contained no alkalinity. This impact is comparable to the TA increase associated with biological NO_3+NO_2 uptake (8 μmol kg^{-1}) that occurred between winter and summer.

nTA at the near-shore site in the present study was higher than the 2299 ± 5 μmol kg^{-1} that has been observed throughout much of the western North Pacific subtropical zone (Takatani et al. 2014) and also higher than the nTA observed in the offshore site at 34°N, 137°E (2296–2315 μmol kg^{-1}; n = 7; JMA 2019) during the same time period. The higher nTA reflects mixing with deeper water above the Suruga trough or Sagami trough, and river runoff as discussed above. According to the survey along 137 °E by

391 JMA (2019), the water column at the northern site is less stratified compared to the
392 southern site because of lower temperature in the surface layer. Therefore, water with
393 higher nTA would be supplied from the deeper layer. In winter, increase of nTA
394 coincided with decrease in salinity (Fig. 5a).

395 Furthermore, nTA increased at a rate of 24.2 μmol kg^{-1} y^{-1} (Table 1) during the 13-
396 month monitoring period from November 2011 to June 2013 (Fig. 4a). We consider that
397 the time course of nTA reflects an increase of mixing with deeper water in latter part of
398 the study period, because nTA increases with depth (Fig. 5a). This is consistent with the
399 finding that temperature was relatively lower in the latter part of the study period (Fig.
400 2a). In addition, the concentration of nDIC was higher in the latter period (Fig. 4b) with
401 a rate of increase of 11.0 μmol kg^{-1} y^{-1} as described below (Table 1).

402 These values of nDIC in the surface layer are comparable to, or about 50 μmol kg^{-1}
403 higher than, those observed at the offshore site (34°N, 137°E) during the same period of
404 time (JMA 2019). When the water was stratified, there was a large vertical gradient of
405 nDIC . These seasonal variations of nDIC at depths of 20 and 30 m were closely related
406 to variations of nutrient concentrations. We calculated the $\Delta nDIC/\Delta n(NO_3+NO_2)$ ratio
407 to be 11.1, using the data from all depths (Fig. 5b). This ratio is significantly higher than
408 the usual stoichiometry of POM (C/N~6.75) (Martiny et al. 2013b). If the dynamics of
409 carbon and nitrogen are controlled by photosynthesis and remineralization, the
410 $\Delta nDIC/\Delta n(NO_3+NO_2)$ ratios should be close to the conventional C/N ratio. In the
411 period from winter to early summer (February to June 2012), steep declines of nDIC
412 and $n(NO_3+NO_2)$ were observed, probably due to uptake by phytoplankton. The
413 $\Delta nDIC/\Delta n(NO_3+NO_2)$ ratio in this period was 8.4, lower than the ratio using all of the
414 data, because biological process mostly control the concentrations of nDIC and
415 $n(NO_3+NO_2)$. Both nDIC and $n(NO_3+NO_2)$ concentrations rapidly increased from late

autumn to winter (November 2011 to January 2012 and November 2012 to January 2013), when DIC and nutrients were supplied by vertical mixing. Using datasets for this period, the ratio of ΔnDIC/Δn(NO_3+NO_2) was 12.8. Higher ΔnDIC/Δn(NO_3+NO_2) are sometimes observed due to production of organic materials with high C/N ratio such as sinking particles and DOM (Sambrotto et al. 1993; Thomas et al. 1999). We should also consider DIC in river runoff. DIC is similar to alkalinity in most rivers (Amiotte Suchet et al. 2003), so we estimate the DIC input from rivers to be +14 μmol kg^{-1} based seasonal change in TA and salinity.

It is also noteworthy that the variations of nDIC in the surface layer were strongly correlated with temperature (Fig. 6a). Even when we compare the temperature and nDIC over shorter periods (<2 months), nDIC was significantly correlated with temperature (Supplementary discussion and Fig. S3). A similar correlation has been observed at an offshore site in the HSCZ (Ishii et al. 2011). nDIC at a given temperature at the near-shore site in our study was similar to or higher than nDIC at the same temperature at 34°N, 137°E (16-26 ºC: 1986-2071 μmol kg^{-1}) (JMA 2019). The relationship between seasonal variations of nDIC versus temperature and Chl *a* was expressed as a quadratic function of temperature (Table 1); inclusion of the *Chl.a* term gave a 0.55 μmol kg^{-1} smaller rms. The regression suggests that nDIC increased during the time of this study at a rate of 11.0 ± 2.4 μmol kg^{-1} yr^{-1} along with the increase of TA at a rate of 24.2 ± 1.7 μmol kg^{-1} $year^{-1}$ (Table 1), probably as a result of the upward movement of deep water. If vertical mixing alone was responsible for the increase of DIC and TA, the carbonate chemistry at our study site would be similar to 34°N, 137°E. However, the ratio of nDIC to pTA increase; 11.0/24.2 ≈ 0.45, was much smaller than the ratio of changes of nDIC and pTA with depth (~3.4) . The reason for this large difference is unclear at the moment, but we speculate that biological production during periods of vertical mixing preferentially reduced DIC

441 in the subsurface water entrained into the mixed layer and thus reduced the vertical
442 gradient of DIC/TA.

443 *4.3. Variation of Ω_{arg} and sensitivity analysis*

444 To quantify the contribution of variations of each of the parameters controlling the
445 variation of Ω_{arg}, we carried out an analysis of the sensitivity of Ω_{arg} to DIC, TA,
446 temperature, and salinity based on the following equation (Hauri et al. 2013):

447 $$\Delta\Omega_{arg} = \frac{\partial\Omega arg}{\partial DIC}\Delta nDIC + \frac{\partial\Omega arg}{\partial TA}\Delta nTA + \frac{\partial\Omega arg}{\partial T}\Delta T + \Delta S_{\Omega arg}, \quad (3)$$

448 where $\Delta\Omega_{arg}$, ΔnDIC, ΔnTA, and ΔT denote the deviations of Ω_{arg}, nDIC, nTA, and
449 temperature, respectively, from their mean values during the study, and the derivatives
450 $\frac{\partial\Omega arg}{\partial DIC}$, $\frac{\partial\Omega arg}{\partial TA}$, and $\frac{\partial\Omega arg}{\partial T}$ were calculated at the mean values of DIC, TA, T, and S. $\Delta S_{\Omega arg}$
451 is the contribution of salinity change to $\Delta\Omega_{arg}$ and can be decomposed as follows:

452 $$\Delta S_{\Omega arg} = \frac{\partial\Omega arg}{\partial S}\Delta S + \frac{\partial\Omega arg}{\partial DIC}\Delta DIC^{s} + \frac{\partial\Omega arg}{\partial TA}\Delta TA^{s}. \quad (4)$$

453 ΔDIC^{s} and ΔTA^{s} represent the effects of dilution on the changes of DIC and TA,
454 respectively.

455 This analysis made it clear that seasonal variations of Ω_{arg} (range of 1.16) was
456 predominantly attributable to variations of DIC at all depths that we investigated (Fig. 7),
457 i.e., the increase of Ω_{arg} in the surface layer in summer, the decrease in winter, and the
458 transient decrease in lower layers during summer were all explained mainly by variation
459 of DIC. However, there were small discrepancies between $\Delta\Omega_{arg}$ and $\frac{\partial\Omega arg}{\partial DIC}\Delta$nDIC that
460 were explained by variations of TA and temperature. For example, $\frac{\partial\Omega arg}{\partial TA}\Delta$nTA at 1 m
461 depth during the study period increased from -0.13 ± 0.08 in the early period from
462 November 2011 to May 2012 to +0.14 ± 0.08 during the later period from December 2012

to June 2013. Therefore, the increase of TA contributed to the elevation of Ω_{arg}. For temperature, $\frac{\partial \Omega arg}{\partial T}\Delta T$ was higher in summer (Jun-Aug 2012: from 0.016 ± 0.017 at 30 m to 0.075 ± 0.031 at 1 m) and lower in winter (Dec 2011 to Feb 2012 and Dec 2012 to Feb 2013: from -0.040 ± 0.026 at 30 m to -0.038 ± 0.028 at 10 m). The range of $\Delta S_{\Omega arg}$ was consistently small (−0.01 to 0.008), so the effect of salinity change on Ω_{arg} was minimal throughout the monitoring period. These seasonal variations were in phase with that of $\frac{\partial \Omega arg}{\partial DIC}\Delta$nDIC induced by biological activity and reinforced the seasonal variations of $\Delta\Omega_{arg}$. Ω_{arg} was maximal in the surface layer in summer, suggesting that favourable conditions for calcareous organisms develop due to consumption of inorganic carbon by phytoplankton.

4.4. Mapping of Ω_{arg} in the surface layer of the HSCZ

In the discussion of pTA and nDIC, we presented empirical models that estimate pTA as a function of time and salinity and nDIC as a function of time, temperature, and chlorophyll *a* concentration (Table 1). These can be used to reconstruct the variations of Ω_{arg} as well as other CO_2 system variables. The residuals of pTA and nDIC were 4.6 and 12.8 μmol kg^{-1} at the near-shore site (Table 1). We also applied these equations to data from the offshore site at 137°E, 34°N in the western HSCZ (JMA 2019). Estimates of TA and DIC at the offshore site were biased by +30 ± 16 and +31 ± 16 μmol kg^{-1} for data collected during the same period. Alternatively, we attempted to estimate Ω_{arg} as a function of the time of sampling, temperature of the seawater, and concentration of chlorophyll—i.e., an equation of the same form as the equation used to estimate nDIC (Table 1)—because the variations of Ω_{arg} were predominantly controlled by variations of nDIC. Figure 6b shows the relationship between Ω_{arg} and temperature. A multiple regression analysis shows that the rate of increase of Ω_{arg} with time was significant (Table

1). This trend is attributable to TA increase, which was twice the rate of DIC increase (Table 1). Such a trend with time should be only applicable for interpolation within the monitoring period in this study (November 2011 to June 2013). Applying these equations to data from 34°N, 137°E (JMA 2019) gave a Ω_{arg} that was biased by only −0.01 ± 0.15. This very small bias implies that the model is applicable throughout the HSCZ during the period of the time-series measurements in this study.

The spatial distributions of Ω_{arg} in the surface layer of the HSCZ were mapped for two seasons, late August 2012 and mid-February 2013 (Fig. 8). The maps were based estimates of Ω_{arg} using satellite derived sea surface temperature (SST) and surface chlorophyll concentrations. We used monthly SST dataset based on the "Merged satellite and in situ data Global Daily Sea Surface Temperatures (MGDSST)" (Kurihara, 2006). In this product, SST from satellite infrared (NOAA/AVHRR, MetOp/AVHRR) and microwave sensors (Coriolis/WINDSAT, GCOM-W1/AMSR-2) is corrected by in situ SST obtained by ships and buoys. SST datasets are available via The North-East Asian Regional GOOS (NEAR-GOOS) website (http://ds.data.jma.go.jp/gmd/goos/data/rrtdb/jma-pro.html). Surface chlorophyll concentrations were estimated using data from the Moderate Resolution Imaging Spectroradiometer (MODIS) instruments aboard NASA's Terra and Aqua satellites; see Hu et al. (2012) for details of the method. Monthly chlorophyll data are available via NASA Earth observations website (https://neo.sci.gsfc.nasa.gov/view.php?datasetId=MY1DMM_CHLORA).

In the region north of 33.3°N, between 135.8°E and 139.9°E, which includes the HSCZ, SST in late August 2012 was generally high (26.7–28.8 °C), and the meridional gradient small. We estimated Ω_{arg} to be 3.4–3.5 over this region. By contrast, during February 2013, SST was relatively low and exhibited a notable meridional gradient from

512 13.9 °C near the coast to 19.0 °C in the Kuroshio. Accordingly, the lowest value of Ω_{arg}
513 (2.5) occurred near the coast, and Ω_{arg} increased southward to 3.1 in the Kuroshio. In
514 general, SST in the HSCZ exhibited a significant meridional gradient in winter, with the
515 coldest water near the coast (JMA 2019). This pattern suggests that the minimum value
516 of Ω_{arg} near the coast and its increase southward toward the Kuroshio is a general
517 characteristic of the surface layer of the HSCZ in winter, although the value of Ω_{arg} is
518 likely to show significant variability during the winter and from year to year in
519 conjunction with the variability of oceanographic conditions.
520 On a long timescale, Ishii et al. (2011) have documented that Ω_{arg} changed at a rate
521 of -0.12 ± 0.05 per decade from 1994 to 2008 at an offshore site (137°E, 33.67–
522 34.00°N) in the western HSCZ. They also projected that, given an intensive fossil fuel
523 use scenario and under colder winter conditions in the HSCZ where the SST is lower
524 than 14.0 °C, Ω_{arg} could decline to 2.0 by 2040, when atmospheric CO_2 is expected to
525 reach 500 ppm. The complex oceanographic conditions in the coastal zone—as
526 exemplified by the TA increase and impact of riverine input found in this study—makes
527 projection of Ω_{arg} more difficult in coastal regions. However, it seems likely that Ω_{arg} in
528 the coastal region will reach threshold values earlier than in the offshore regions near
529 the Kuroshio, and the impact on marine ecosystems will be manifested earlier.
530 Since the coastal zone in HSCZ has been known as a biodiversity hotspot (Kerswell
531 2006; Tittensor et al. 2010) and refugium for corals under global warming (Yamano et
532 al. 2011; Makino et al. 2014), a previous study tried to project Ω_{arg} around Japanese
533 coast (Yara et al. 2012). However, the spatial and temporal resolutions in their study
534 were coarse (1°×1° and annual mean). Although our study only covered the HSCZ, the
535 estimates of Ω_{arg} are more precise than those of Yara et al. (2012), and will be helpful
536 for projection of ecosystem change with ocean acidification in the HSCZ.

Acknowledgements

We are grateful to all members of the staff of the Shimoda Marine Research Center for their valuable assistance during the times-series measurements. In particular, we thank technical staff members Mr. Y. Tsuchiya, Mr. T. Sato, H. Shinagawa, and Y. Yamada for their skillful support in the field sampling. This study was financially supported by the Japanese Association for Marine Biology (JAMBIO), grants from the Ministry of Education, Culture, Sports, Science, and Technology, Japan (242410101), and the Global Environmental Research Fund of the Ministry of the Environment, Japan.

546 **References**

547 Albright R, Langdon C, Anthony KRN (2013) Dynamics of seawater carbonate chemistry,
548 production, and calcification of a coral reef flat, central Great Barrier Reef.
549 Biogeosciences 10:6747–6758. https://doi.org/10.5194/bg-10-6747-2013

550 Amiotte Suchet P, Probst J-L, Ludwig W (2003) Worldwide distribution of continental
551 rock lithology: Implications for the atmospheric/soil CO_2 uptake by continental
552 weathering and alkalinity river transport to the oceans: Global Biogeochemical
553 Cycles 17:n/a-n/a. https://doi.org/10.1029/2002GB001891

554 Anthony KRN, Kline DI, Diaz-Pulido G, et al (2008) Ocean acidification causes
555 bleaching and productivity loss in coral reef builders. Proceedings of the National
556 Academy of Sciences 105:17442–17446.
557 https://doi.org/10.1073/pnas.0804478105

558 Ara K, Fukuyama S, Tashiro M, Hiromi J (2011) Seasonal and year-on-year variability in
559 chlorophyll *a* and microphytoplankton assemblages for 9 years (2001–2009) in
560 the neritic area of Sagami Bay, Japan. Plankton and Benthos Research 6:158–174.
561 https://doi.org/10.3800/pbr.6.158

562 Ara K, Hiromi J (2008) Temporal variability and characterization of physicochemical
563 properties in the neritic area of Sagami Bay, Japan. Journal of Oceanography
564 64:195–210. https://doi.org/10.1007/s10872-008-0015-3

565 Baki MA, Motegi C, Shibata A, et al (2009) Temporal changes in chlorophyll *a*
566 concentrations and bacterial, viral, and heterotrophic nanoflagellate abundances
567 in the coastal zone of Sagami Bay, Japan: implications of top-down and bottom-

568 up effects. Coastal Marine Science 33:29–38

569 Barkley RA (1970) The Kuroshio current. Science Journal 6:54–60

570 Bode A, Castro CG, Doval MD, Varela M (2002) New and regenerated production and
571 ammonium regeneration in the western Bransfield Strait region (Antarctica)
572 during phytoplankton bloom conditions in summer. Deep Sea Research Part II:
573 Topical Studies in Oceanography 49:787–804. https://doi.org/10.1016/S0967-
574 0645(01)00124-2

575 Brewer PG, Goldman JC (1976) Alkalinity changes generated by phytoplankton growth1.
576 Limnology and Oceanography 21:108–117.
577 https://doi.org/10.4319/lo.1976.21.1.0108

578 Britton D, Cornwall CE, Revill AT, et al (2016) Ocean acidification reverses the positive
579 effects of seawater pH fluctuations on growth and photosynthesis of the habitat-
580 forming kelp, *Ecklonia radiata*. Scientific Reports 6:.
581 https://doi.org/10.1038/srep26036

582 Caldeira K, Wickett ME (2003) Anthropogenic carbon and ocean pH. Nature 425:365–
583 365. https://doi.org/10.1038/425365a

584 Ciais P, Chris S, Govindasamy B, et al (2013) Carbon and other biogeochemical cycles.
585 Climate Change 2013: The Physical Science Basis 465–570

586 Cornwall CE, Hepburn CD, McGraw CM, et al (2013) Diurnal fluctuations in seawater
587 pH influence the response of a calcifying macroalga to ocean acidification.
588 Proceedings of the Royal Society B: Biological Sciences 280:20132201–
589 20132201. https://doi.org/10.1098/rspb.2013.2201

590 Dickson AG, Sabine CL, Christian JR (2007) Guide to Best Practices for Ocean CO_2
591 Measurements. North Pacific Marine Science Organization

592 Doney SC, Fabry VJ, Feely RA, Kleypas JA (2009) Ocean Acidification: The Other CO_2
593 Problem. Annual Review of Marine Science 1:169–192.
594 https://doi.org/10.1146/annurev.marine.010908.163834

595 Dumousseaud C, Achterberg EP, Tyrrell T, et al (2010) Contrasting effects of temperature
596 and winter mixing on the seasonal and inter-annual variability of the carbonate
597 system in the Northeast Atlantic Ocean. Biogeosciences 7:1481–1492.
598 https://doi.org/10.5194/bg-7-1481-2010

599 Eberlein T, Wohlrab S, Rost B, et al (2017) Effects of ocean acidification on primary
600 production in a coastal North Sea phytoplankton community. PLOS ONE
601 12:e0172594. https://doi.org/10.1371/journal.pone.0172594

602 Fabry VJ, Seibel BA, Feely RA, Orr JC (2008) Impacts of ocean acidification on marine
603 fauna and ecosystem processes. ICES Journal of Marine Science 65:414–432.
604 https://doi.org/10.1093/icesjms/fsn048

605 Foltz GR (2003) Seasonal mixed layer heat budget of the tropical Atlantic Ocean. Journal
606 of Geophysical Research 108:. https://doi.org/10.1029/2002JC001584

607 Gong X, Shi J, Gao HW, Yao XH (2015) Steady-state solutions for subsurface chlorophyll
608 maximum in stratified water columns with a bell-shaped vertical profile of
609 chlorophyll. Biogeosciences 12:905–919. https://doi.org/10.5194/bg-12-905-
610 2015

611 Hagiwara N, Senga Y, Niki M, Sugimoto T (2011) Appearance Characteristics of

612 Coccolithphores in Suruga Bay. Journal of Japan Society of Civil Engineers, Ser
613 B2 (Coastal Engineering) 67:I_871-I_875.
614 https://doi.org/10.2208/kaigan.67.I_871

615 Hall-Spencer JM, Rodolfo-Metalpa R, Martin S, et al (2008) Volcanic carbon dioxide
616 vents show ecosystem effects of ocean acidification. Nature 454:96–99.
617 https://doi.org/10.1038/nature07051

618 Hama T, Inoue T, Suzuki R, et al (2016) Response of a phytoplankton community to
619 nutrient addition under different CO_2 and pH conditions. Journal of Oceanography
620 72:207–223. https://doi.org/10.1007/s10872-015-0322-4

621 Hama T, Kawashima S, Shimotori K, et al (2012) Effect of ocean acidification on coastal
622 phytoplankton composition and accompanying organic nitrogen production.
623 Journal of Oceanography 68:183–194. https://doi.org/10.1007/s10872-011-0084-
624 6

625 Hansen HP, Koroleff F (2007) Determination of nutrients. In: Methods of Seawater
626 Analysis. John Wiley & Sons, Ltd, pp 159–228

627 Hauri C, Gruber N, Vogt M, et al (2013) Spatiotemporal variability and long-term trends
628 of ocean acidification in the California Current System. Biogeosciences 10:193–
629 216. https://doi.org/10.5194/bg-10-193-2013

630 Hofmann GE, Smith JE, Johnson KS, et al (2011) High-Frequency Dynamics of Ocean
631 pH: A Multi-Ecosystem Comparison. PLOS ONE 6:e28983.
632 https://doi.org/10.1371/journal.pone.0028983

633 Hu C, Lee Z, Franz B (2012) Chlorophyll *a* algorithms for oligotrophic oceans: A novel

634 approach based on three-band reflectance difference. Journal of Geophysical
635 Research: Oceans 117:. https://doi.org/10.1029/2011JC007395

636 IPCC (2013) Climate change 2013: The Physical Science Basis. Contribution of Working
637 Group I to the Fifth Assessment Report of the Intergovernmental Panel on Climate
638 Change. https://www.ipcc.ch/report/ar5/wg1/. Accessed 10 Jan 2019

639 Ishii M, Inoue HY, Matsueda H, et al (2001) Seasonal variation in total inorganic carbon
640 and its controlling processes in surface waters of the western North Pacific
641 subtropical gyre. Marine Chemistry 75:17–32. https://doi.org/10.1016/S0304-
642 4203(01)00023-8

643 Ishii M, Kosugi N, Sasano D, et al (2011) Ocean acidification off the south coast of Japan:
644 A result from time series observations of CO_2 parameters from 1994 to 2008.
645 Journal of Geophysical Research 116:. https://doi.org/10.1029/2010JC006831

646 Jiang Z-P, Tyrrell T, Hydes DJ, et al (2014) Variability of alkalinity and the alkalinity-
647 salinity relationship in the tropical and subtropical surface ocean. Global
648 Biogeochemical Cycles 28:729–742. https://doi.org/10.1002/2013GB004678

649 JMA (2019) Japan Meteorological Agency | Data of Oceanographic and Marine
650 Meteorological Observation | Oceanographic Section Time-series Dataset in the
651 137°E Section.
652 http://www.data.jma.go.jp/gmd/kaiyou/db/mar_env/results/OI/137E_OI_e.html.
653 Accessed 4 Jul 2019

654 Kai M, Hara T, Aoyama H, Kuroda N (1999) A Massive Coccolithophorid Bloom
655 Observed in Mikawa Bay, Japan. Journal of Oceanography 55:395–406.

https://doi.org/10.1023/A:1007806500053

Kamatani A, Ogura N, Nakamoto N, et al (1981) Distribution of nutrients in Sagami Bay during 1971-1973. NIPPON SUISAN GAKKAISHI 47:1493–1498. https://doi.org/10.2331/suisan.47.1493

Kamatani A, Oku O, Maeda M, Yamada Y (2000) The Distribution and Fate of Nutrients in Sagami Bay. NIPPON SUISAN GAKKAISHI 66:70–79

Kerswell AP (2006) Global biodiversity patterns of benthic marine algae. Ecology 87:2479–2488. https://doi.org/10.1890/0012-9658(2006)87[2479:GBPOBM]2.0.CO;2

Kinoshita J, Kon I, Miyahara T (2002) Characteristics of Nutritional Variations in the Odawara Sea Area of the Sagami Bay Deep Seawater. Deep Ocean Water Research 3:7–13

Kroeker KJ, Kordas RL, Crim R, et al (2013) Impacts of ocean acidification on marine organisms: quantifying sensitivities and interaction with warming. Global Change Biology 19:1884–1896. https://doi.org/10.1111/gcb.12179

Kurihara Y (2006) Global daily sea surface temperature analysis using data from satellite microwave radiometer, satellite infrared radiometer and in-situ observations. Weather Service Bulletin 73:s1–s18

Le Quéré C, Peters GP, Andres RJ, et al (2014) Global carbon budget 2013. Earth System Science Data 6:235–263. https://doi.org/10.5194/essd-6-235-2014

Lueker TJ, Dickson AG, Keeling CD (2000) Ocean pCO_2 calculated from dissolved

677 inorganic carbon, alkalinity, and equations for K1 and K2: validation based on
678 laboratory measurements of CO_2 in gas and seawater at equilibrium. Marine
679 Chemistry 70:105–119. https://doi.org/10.1016/S0304-4203(00)00022-0

680 Makino A, Yamano H, Beger M, et al (2014) Spatio-temporal marine conservation
681 planning to support high-latitude coral range expansion under climate change.
682 Diversity and Distributions 20:859–871. https://doi.org/10.1111/ddi.12184

683 Martiny AC, Pham CTA, Primeau FW, et al (2013a) Strong latitudinal patterns in the
684 elemental ratios of marine plankton and organic matter. Nature Geoscience 6:279–
685 283. https://doi.org/10.1038/ngeo1757

686 Martiny AC, Vrugt JA, Primeau FW, Lomas MW (2013b) Regional variation in the
687 particulate organic carbon to nitrogen ratio in the surface ocean: upper ocean C:N
688 ratio. Global Biogeochemical Cycles 27:723–731.
689 https://doi.org/10.1002/gbc.20061

690 McNeil BI, Matear RJ (2008) Southern Ocean acidification: A tipping point at 450-ppm
691 atmospheric CO_2. Proceedings of the National Academy of Sciences 105:18860–
692 18864. https://doi.org/10.1073/pnas.0806318105

693 Michaelidis B, Spring A, Pörtner HO (2007) Effects of long-term acclimation to
694 environmental hypercapnia on extracellular acid–base status and metabolic
695 capacity in Mediterranean fish Sparus aurata. Marine Biology 150:1417–1429.
696 https://doi.org/10.1007/s00227-006-0436-8

697 Mie Prefectural Government (2014) Engan Teisen Kansoku.
698 http://www.pref.mie.lg.jp/common/05/ci600012645.htm. Accessed 7 Jan 2019

699 Miyaguchi H, Fujiki T, Kikuchi T, et al (2006) Relationship between the bloom of
700 *Noctiluca scintillans* and environmental factors in the coastal waters of Sagami
701 Bay, Japan. Journal of Plankton Research 28:313–324.
702 https://doi.org/10.1093/plankt/fbi127

703 Miyashita M (2005) Bi-weekly to Seasonal Variability of Satellite-derived Chlorophyll *a*
704 Distribution: Controlling Factors in the Ocean South of Honshu Island. Journal of
705 The Remote Sensing Society of Japan 25:169–178.
706 https://doi.org/10.11440/rssj1981.25.169

707 Mucci A (1983) The solubility of calcite and aragonite in seawater at various salinities,
708 temperatures, and one atmosphere total pressure. American Journal of Science
709 283:780–799. https://doi.org/10.2475/ajs.283.7.780

710 Omote J, Hatanaka T (2011) Determination of fluorescence Chlorophyll *a* concentration
711 in Kumanonada bays. Research reports Kinki University Technical 69–77

712 Pierrot, Wallace, Lewis, et al (2011) MS Excel Program Developed for CO_2 System
713 Calculations. https://doi.org/10.3334/cdiac/otg.co2sys_xls_cdiac105a

714 Pörtner HO, Langenbuch M, Reipschläger A (2004) Biological Impact of Elevated Ocean
715 CO_2 Concentrations: Lessons from Animal Physiology and Earth History. Journal
716 of Oceanography 60:705–718. https://doi.org/10.1007/s10872-004-5763-0

717 Prentice IC, Farquhar GD, Fasham MJR, et al (2001) The Carbon Cycle and Atmospheric
718 Carbon Dioxide — IPCC. In: Climate Change 2001: the Scientific Basis.
719 Contributions of Working Group I to the Third Assessment Report of the
720 Intergovernmental Panel on Climate Change. Cambridge University Press

721 R Core Team (2018) R: The R Project for Statistical Computing. https://www.r-
722 project.org/. Accessed 31 Dec 2018

723 Riebesell U, Schulz KG, Bellerby RGJ, et al (2007) Enhanced biological carbon
724 consumption in a high CO_2 ocean. Nature 450:545–548.
725 https://doi.org/10.1038/nature06267

726 Rivest EB, Hofmann GE (2014) Responses of the Metabolism of the Larvae of
727 *Pocillopora damicornis* to Ocean Acidification and Warming. PLOS ONE
728 9:e96172. https://doi.org/10.1371/journal.pone.0096172

729 Saito S, Ishii M, Midorikawa T (2008) Precise Spectrophotometric Measurement of
730 Seawater pH_T with an Automated Apparatus using a Flow Cell in a Closed Circuit.
731 Technical Reports of the MRI 57:

732 Sambrotto RN, Savidge G, Robinson C, et al (1993) Elevated consumption of carbon
733 relative to nitrogen in the surface ocean. Nature 363:248–250.
734 https://doi.org/10.1038/363248a0

735 Sassa C, Kawaguchi K, Oozeki Y, et al (2004) Distribution patterns of larval myctophid
736 fishes in the transition region of the western North Pacific. Marine Biology
737 144:417–428. https://doi.org/10.1007/s00227-003-1214-5

738 Schneider A, Wallace DWR, Körtzinger A (2007) Alkalinity of the Mediterranean Sea.
739 Geophysical Research Letters 34:. https://doi.org/10.1029/2006GL028842

740 Sugisaki H, Nonaka M, Isizaki S, et al (2010) Status and trends of the Kuroshio region,
741 2003-2008. North Pacific Marine Science Organization, Sydney, B.C., Canada

742 Taguchi F, Fujiwara T, Yamada Y, et al (2009) Alkalinity in coastal seas around Japan.
743 Bulletin on Coastal Oceanography 47:71–75

744 Takatani Y, Enyo K, Iida Y, et al (2014) Relationships between total alkalinity in surface
745 water and sea surface dynamic height in the Pacific Ocean. Journal of Geophysical
746 Research: Oceans 119:2806–2814. https://doi.org/10.1002/2013JC009739

747 Thomas H, Ittekkot V, Osterroht C, Schneider B (1999) Preferential recycling of
748 nutrients-the ocean's way to increase new production and to pass nutrient
749 limitation? Limnology and Oceanography 44:1999–2004.
750 https://doi.org/10.4319/lo.1999.44.8.1999

751 Tittensor DP, Mora C, Jetz W, et al (2010) Global patterns and predictors of marine
752 biodiversity across taxa. Nature 466:1098–1101.
753 https://doi.org/10.1038/nature09329

754 Urakawa LS, Kurogi M, Yoshimura K, Hasumi H (2015) Modeling low salinity waters
755 along the coast around Japan using a high-resolution river discharge dataset.
756 Journal of Oceanography 71:715–739. https://doi.org/10.1007/s10872-015-0314-
757 4

758 Veron JEN, Minchin PR (1992) Correlations between sea surface temperature, circulation
759 patterns and the distribution of hermatypic corals of Japan. Continental Shelf
760 Research 12:835–857. https://doi.org/10.1016/0278-4343(92)90047-N

761 WMO (2016) WMO WDCGG (World Data Centre for Greenhous Gases) Data Summary,
762 41. https://gaw.kishou.go.jp/publications/summary. Accessed 8 Jan 2019

763 Yamano H, Sugihara K, Nomura K (2011) Rapid poleward range expansion of tropical

764 reef corals in response to rising sea surface temperatures. Geophysical Research
765 Letters 38:. https://doi.org/10.1029/2010GL046474

766 Yao W, Byrne RH (1998) Simplified seawater alkalinity analysis: Use of linear array
767 spectrometers. Deep Sea Research Part I: Oceanographic Research Papers
768 45:1383–1392. https://doi.org/10.1016/S0967-0637(98)00018-1

769 Yara Y, Vogt M, Fujii M, et al (2012) Ocean acidification limits temperature-induced
770 poleward expansion of coral habitats around Japan. Biogeosciences 9:4955–4968.
771 https://doi.org/10.5194/bg-9-4955-2012

772 Yokouchi K, Tsuda A, Kuwata A, et al (2007) Chapter 3 Simulated In Situ Measurements
773 of Primary Production in Japanese Waters. In: Kawahata H, Awaya Y (eds)
774 Elsevier Oceanography Series. Elsevier, pp 65–480

775

776

777 **Figure captions**

778 **Fig. 1.** Map of the Honshu South Coastal Zone and location of the sampling station.
779 The units of the depth contours are meters.

780

781 **Fig. 2.** Time series of (a) temperature profiles (°C), (b) mixed layer depths (m), (c)
782 salinity profiles, and (d) chlorophyll *a* concentration profiles (mg m^{-3}) from November
783 2011 to June 2013. Arrows above panel (a) indicate sampling dates for panels (a-d). In
784 the panel (b), solid circles mean the mixed layer depths, and open ones imply that mixed
785 layer depth was not identified because variation of temperature along depth was within
786 0.5 °C.

787

788 **Fig. 3.** Time series of (a) NO_2+NO_3 profiles, (b) PO_4 profiles, and (c) NH_4 profiles
789 (μM) from November 2011 to March 2013. Arrows above panel (a) indicate the date of
790 sampling for all panels. Data are lacking after late March 2013.

791

792 **Fig. 4.** Time series of profiles of (a) total alkalinity normalized to a salinity of 35 (μmol
793 kg^{-1}) (nTA), (b) total dissolved inorganic carbon normalized to a salinity of 35 (μmol
794 kg^{-1}) (nDIC) and (c) aragonite saturation index (Ω_{arg}) from November 2011 to June
795 2013. Arrows above panel (a) indicate the date of sampling for all panels.

796

797 **Fig. 5.** Relationship between (a) total alkalinity (TA) versus salinity in the upper layer
798 (1 and 10 m), and (b) salinity-normalized DIC versus nitrate+nitrite concentrations
799 (nDIC vs nNO_3+NO_2) at the station off Shimoda during the period from November
800 2011 to June 2013 (filled circles). Open squares show the data at 34°N, 137°E for the

801 same period (JMA 2019). In the panel (a), data in the top 700 m was shown, while only
802 data in surface was shown in the panel (b) (JMA 2019).
803
804 **Fig. 6.** Relationships of (a) total dissolved inorganic carbon normalized to a salinity of
805 35 (nDIC) versus temperature and (b) aragonite saturation index (Ω_{arg}) versus
806 temperature in the upper layer (1 and 10 m) at the station off Shimoda for the period
807 from November 2011 to June 2013 (filled circles) and in surface layer (0 m) at 34°N,
808 137°E for the same period (open square) (JMA 2019).
809
810 **Fig. 7.** Results of the sensitivity analysis for the changes in $\Delta\Omega_{arg}$ versus changes of
811 nDIC, nTA, temperature, and salinity. Time series of $\Delta\Omega_{arg}$ (●), $\frac{\partial\Omega arg}{\partial DIC}\Delta$nDIC (○),
812 $\frac{\partial\Omega arg}{\partial TA}\Delta$nTA (■), $\frac{\partial\Omega arg}{\partial T}\Delta$T (□), and $\Delta S_{\Omega arg}$ (▲) for depths of (a) 1 m, (b) 10 m, (c) 20 m,
813 and (d) 30 m during the period from November 2011 to June 2013. Arrows above figure
814 indicate sampling dates.
815
816 **Fig. 8.** Maps of Ω_{arg} in the surface layer of the Honshu South Coastal Zone in (a) August
817 2012 and (b) February 2013. In February 2013, the path of the Kuroshio was closer to the
818 southern tip of the Izu Peninsula.
819

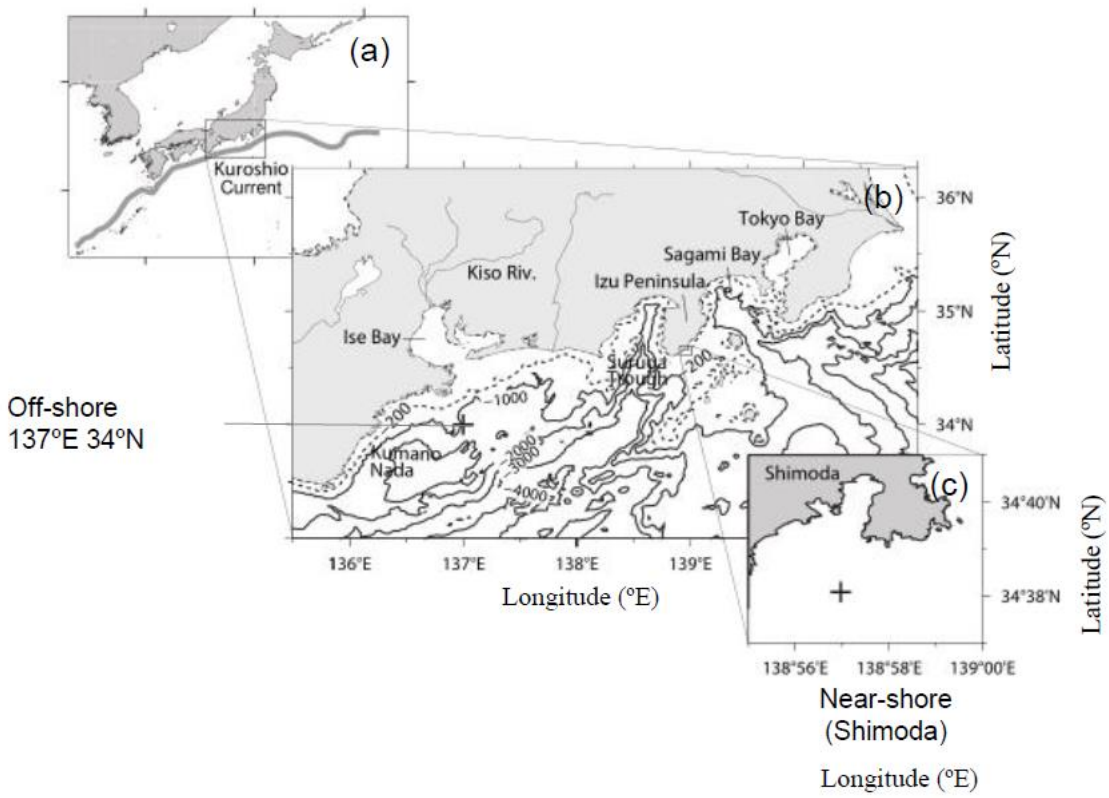
(a)
Kuroshio Current
(b)
Tokyo Bay
Sagami Bay
Kiso Riv.
Izu Peninsula
Ise Bay
Suruga Trough
Kumano Nada
200
1000
2000
3000
4000
36°N
35°N
34°N
Latitude (°N)
136°E
137°E
138°E
139°E
Longitude (°E)
Off-shore
137°E 34°N
Shimoda
(c)
34°40'N
34°38'N
Latitude (°N)
138°56'E
138°58'E
139°00'E
Near-shore
(Shimoda)
Longitude (°E)

820

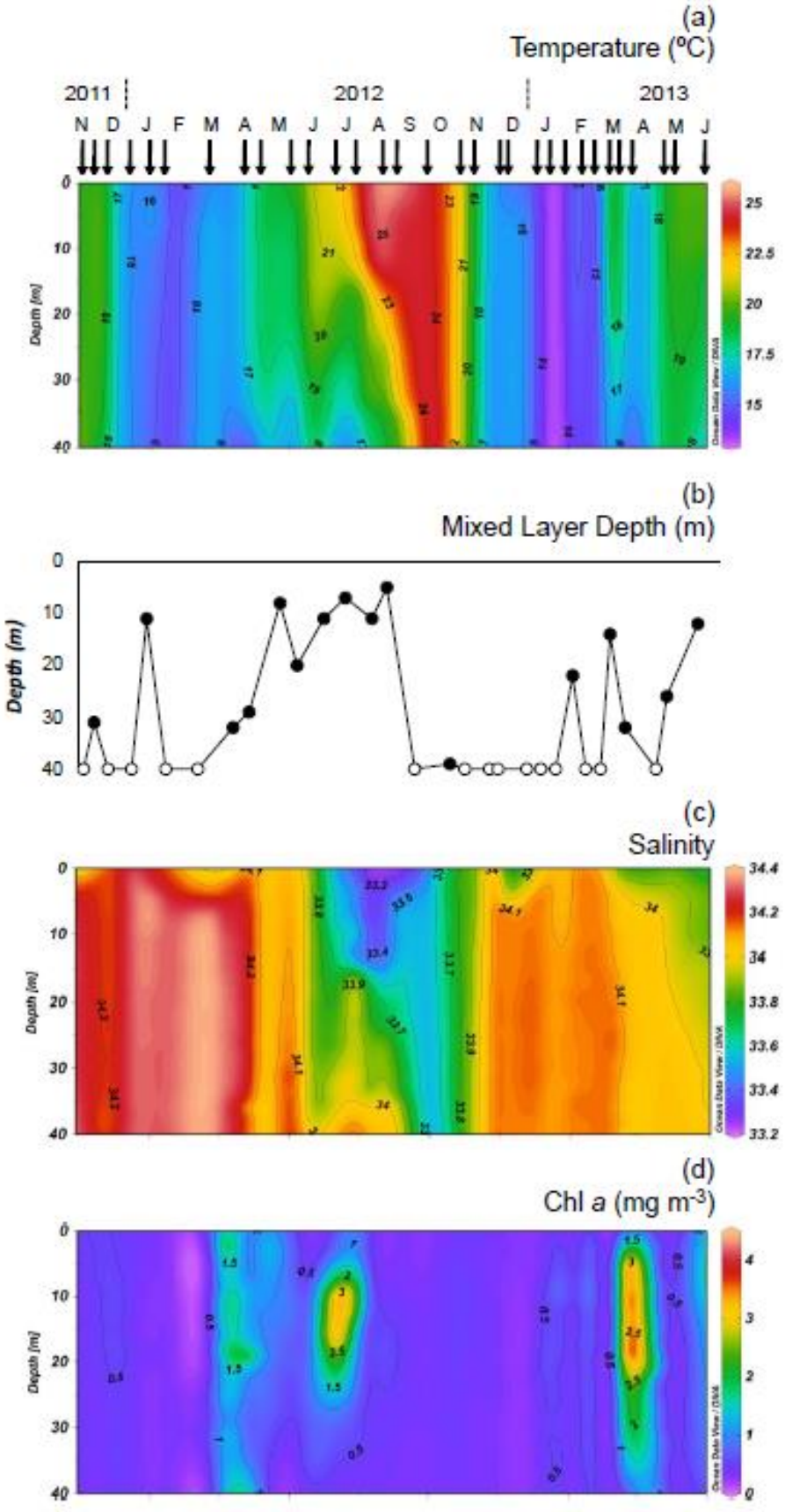
(a)
Temperature (ºC)
2011
2012
2013
N D J F M A M J J A S O N D J F M A M J
Depth (m)
0
10
20
30
40
25
22.5
20
17.5
15
(b)
Mixed Layer Depth (m)
Depth (m)
0
10
20
30
40
(c)
Salinity
Depth (m)
34.4
34.2
34
33.8
33.6
33.4
33.2
(d)
Chl a (mg m-3)
Depth (m)
4
3
2
1
0

821

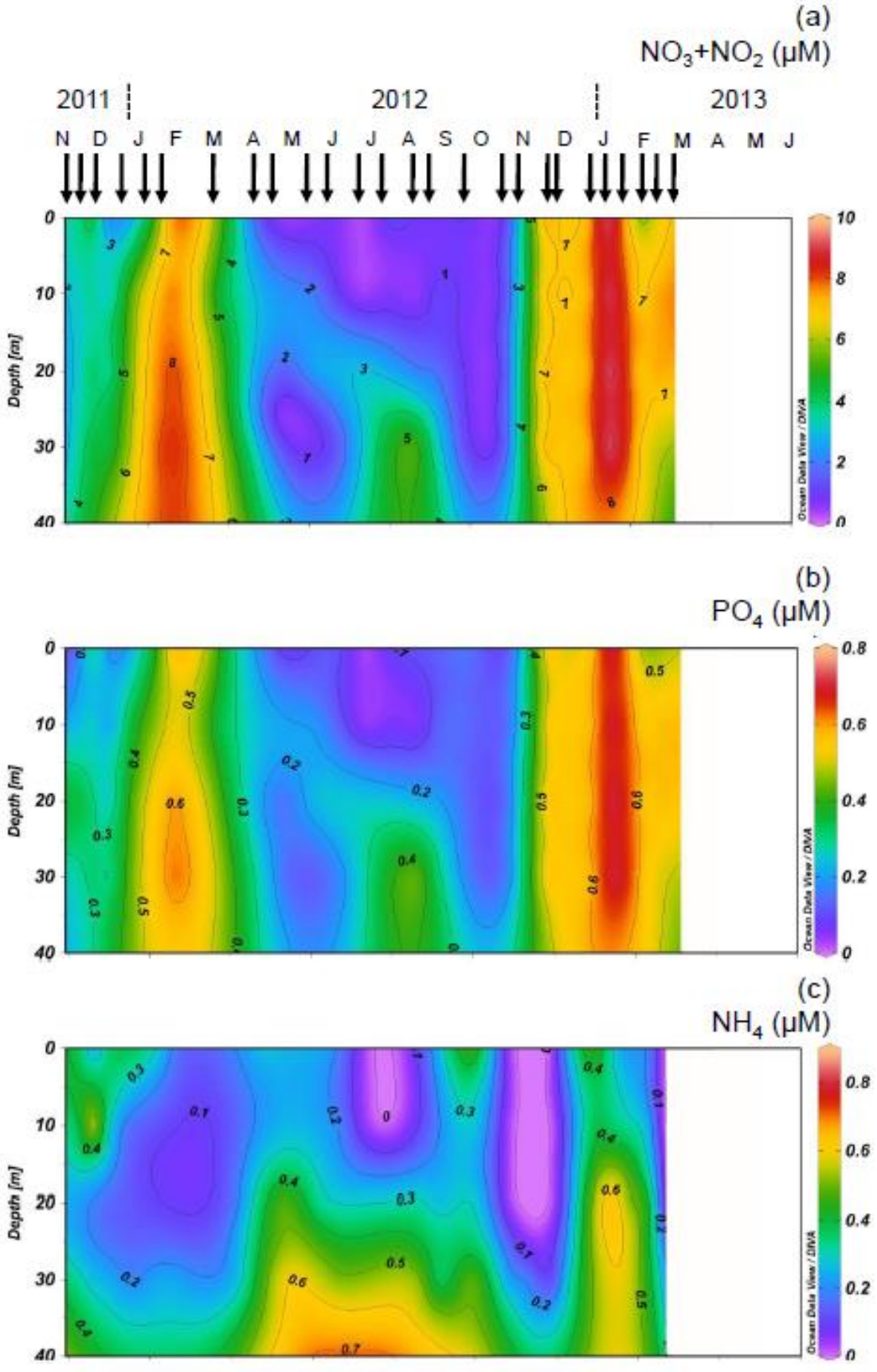
(a)
NO_3+NO_2 (μM)
2011
2012
2013
N D J F M A M J J A S O N D J F M A M J
Depth [m]
0
10
20
30
40
Ocean Data View / DIVA
(b)
PO_4 (μM)
(c)
NH_4 (μM)

822

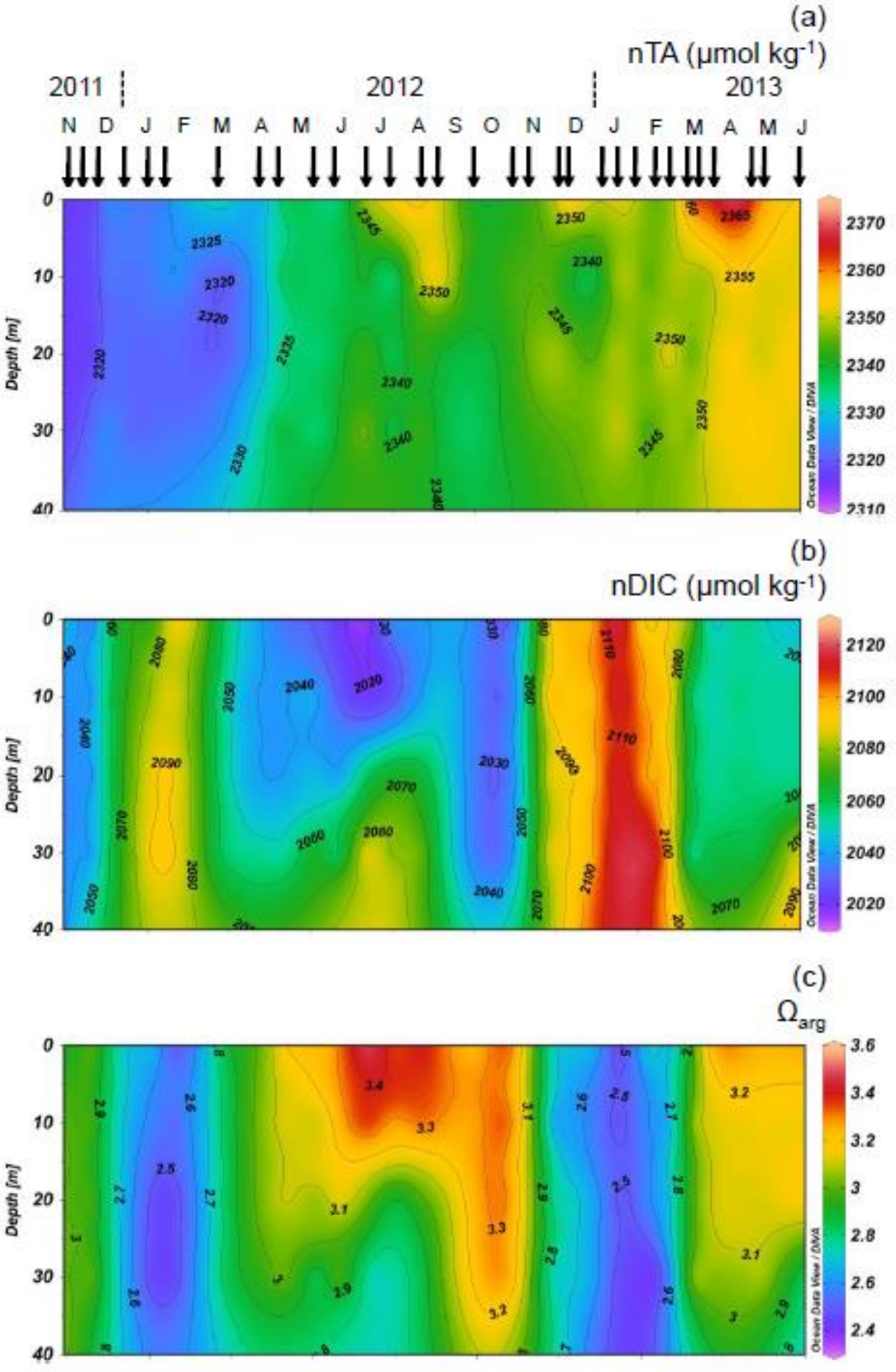
(a)
nTA (µmol kg-1)
2011
2012
2013
N D J F M A M J J A S O N D J F M A M J
Depth [m]
0
10
20
30
40
2370
2360
2350
2340
2330
2320
2310
Ocean Data View / DIVA
(b)
nDIC (µmol kg-1)
2120
2100
2080
2060
2040
2020
(c)
Ωarg
3.6
3.4
3.2
3
2.8
2.6
2.4

823

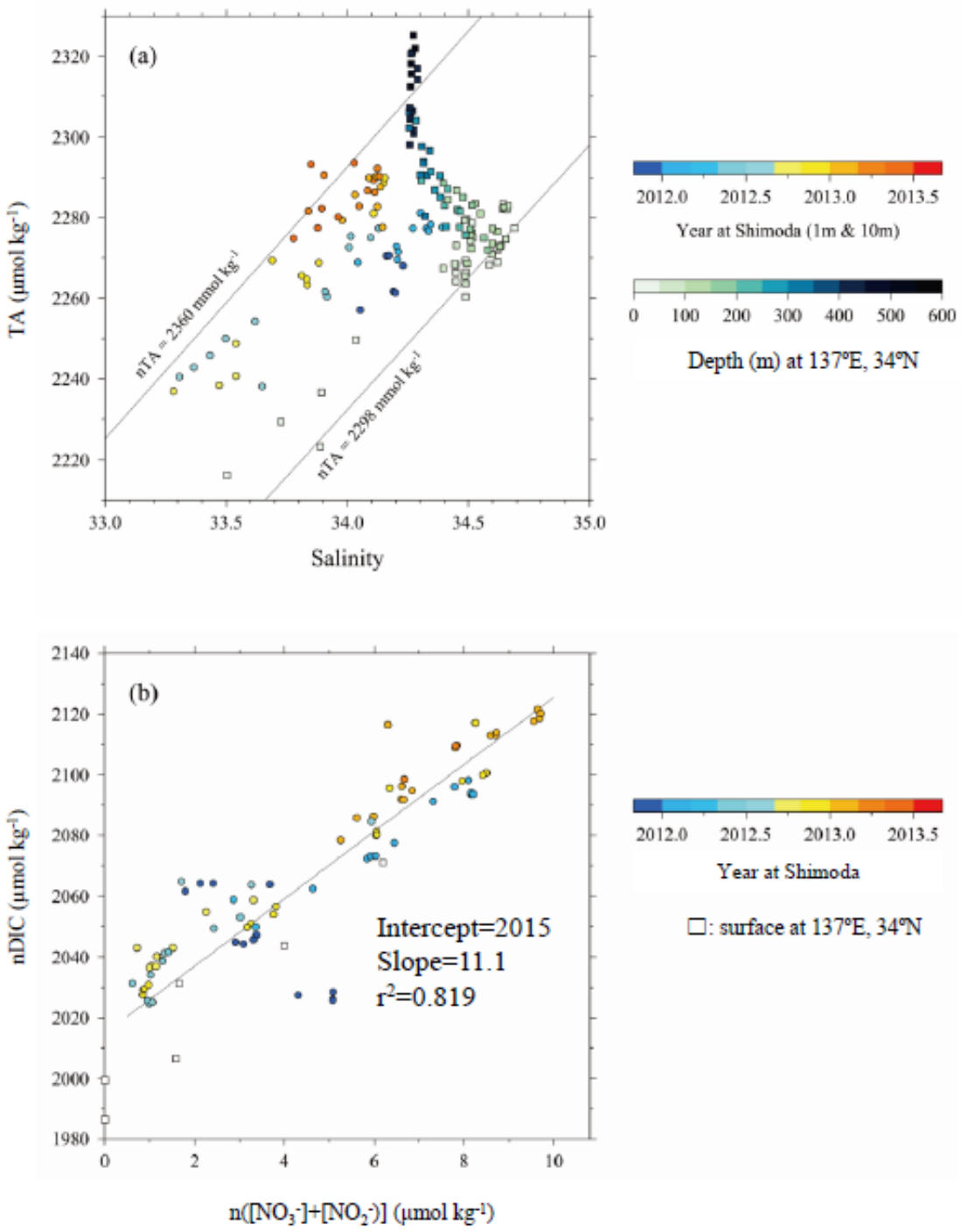
(a)
TA (μmol kg⁻¹)
Salinity
nTA = 2360 mmol kg⁻¹
nTA = 2298 mmol kg⁻¹
2012.0
2012.5
2013.0
2013.5
Year at Shimoda (1m & 10m)
0
100
200
300
400
500
600
Depth (m) at 137°E, 34°N
(b)
nDIC (μmol kg⁻¹)
n([NO3-]+[NO2-)] (μmol kg-1)
Intercept=2015
Slope=11.1
r2=0.819
Year at Shimoda
□: surface at 137°E, 34°N

824

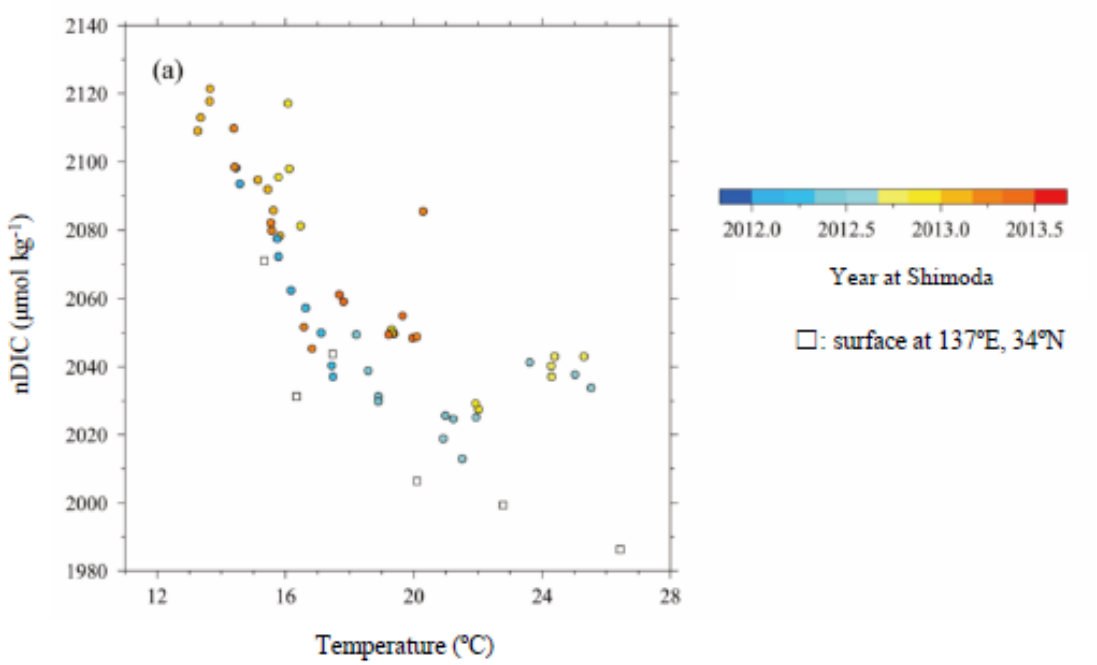
(a)
nDIC (μmol kg⁻¹)
2140
2120
2100
2080
2060
2040
2020
2000
1980
12
16
20
24
28
Temperature (°C)
2012.0
2012.5
2013.0
2013.5
Year at Shimoda
□: surface at 137°E, 34°N

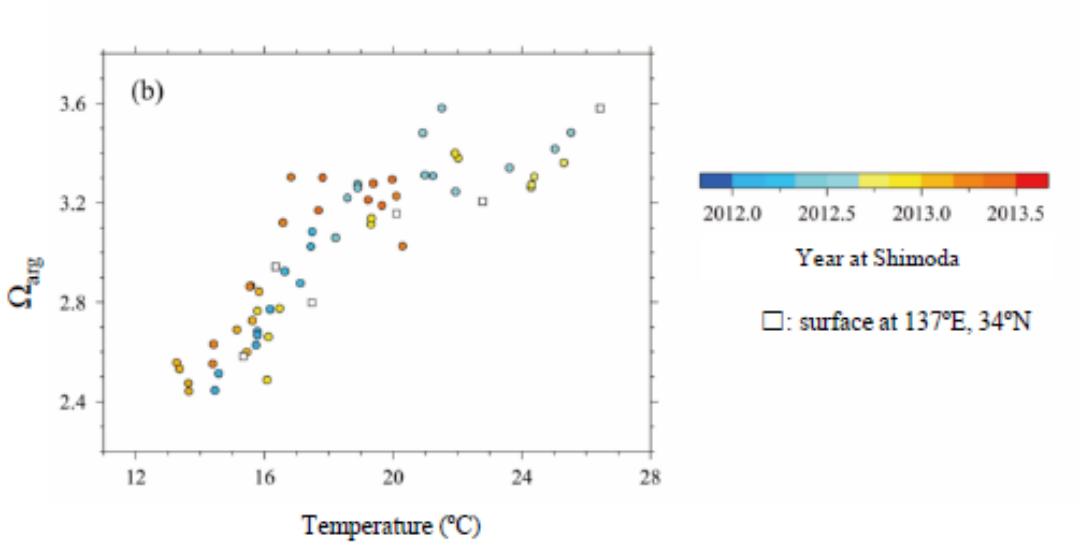
(b)
Ω_{arg}
3.6
3.2
2.8
2.4
12
16
20
24
28
Temperature (°C)
2012.0
2012.5
2013.0
2013.5
Year at Shimoda
□: surface at 137°E, 34°N

825

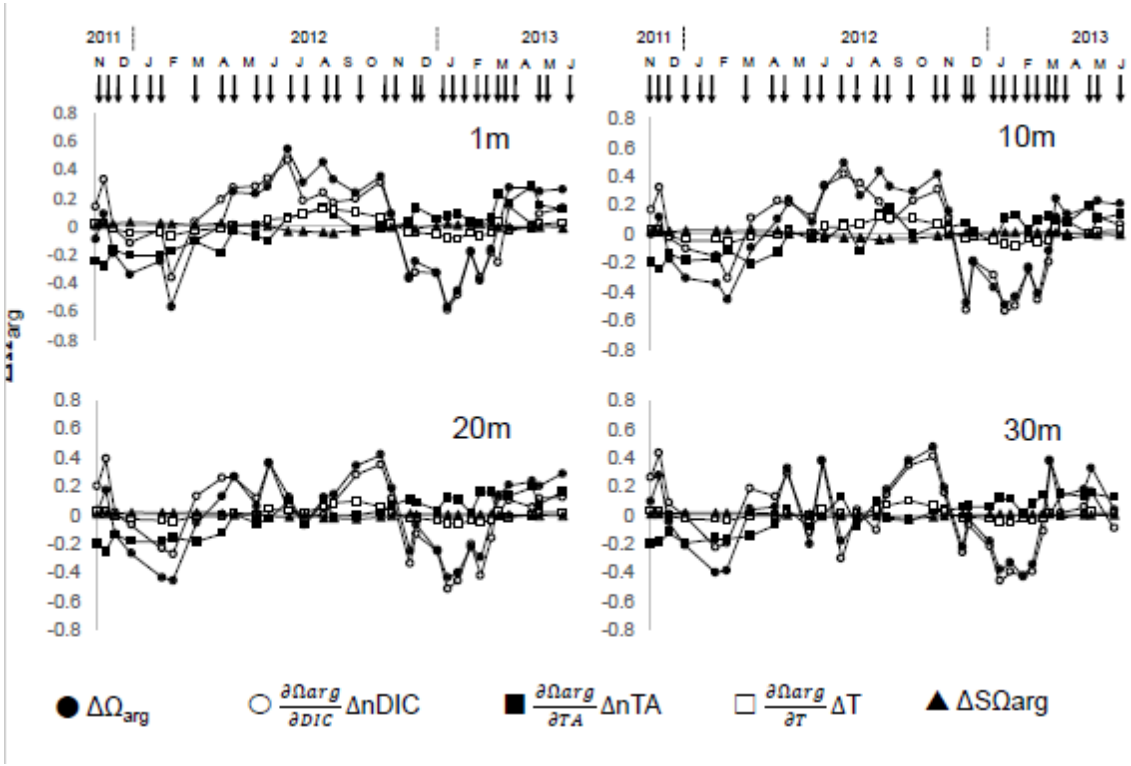
2011
2012
2013
N D J F M A M J J A S O N D J F M A M J
1m
10m
20m
30m
0.8
0.6
0.4
0.2
0
-0.2
-0.4
-0.6
-0.8
● ΔΩarg
○ ∂Ωarg/∂DIC ΔnDIC
■ ∂Ωarg/∂TA ΔnTA
□ ∂Ωarg/∂T ΔT
▲ ΔSΩarg

826

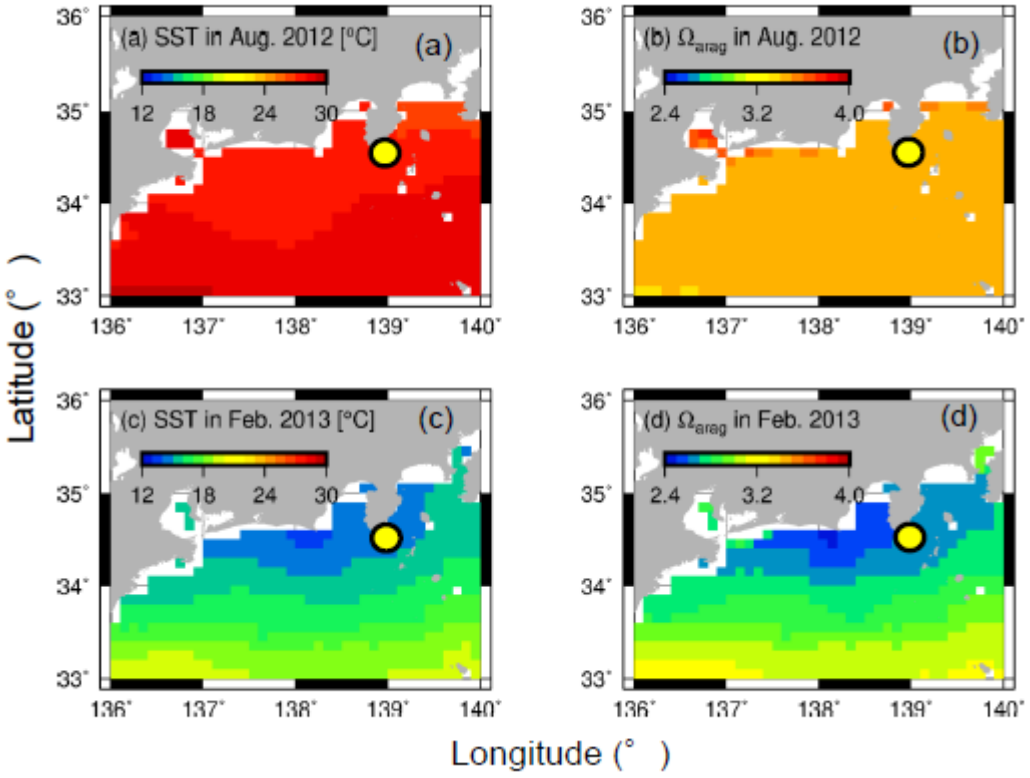
(a) SST in Aug. 2012 [°C]
(a)
12 18 24 30
(b) Ωarag in Aug. 2012
(b)
2.4 3.2 4.0
(c) SST in Feb. 2013 [°C]
(c)
12 18 24 30
(d) Ωarag in Feb. 2013
(d)
2.4 3.2 4.0
36° 35° 34° 33°
136° 137° 138° 139° 140°
Latitude (°)
Longitude (°)

827

828 Table 1 Equations for multi linear regression

Equation	rms of ε
pTA (μmol kg^{-1}) = 506 (± 85) + 52.3 (± 2.5) S + 24.2 (± 1.7) yr + ε_1	4.6
nDIC (μmol kg^{-1}) = 2506.2 (± 40.3) + 11.0 (± 2.4) yr – 40.39 (± 4.36) t + 0.882 (± 0.114) t^2 – 6.888 (± 2.049) *Chl a* + ε_2	12.8
Ω_{arg} = 2.98 (± 0.02) + 0.11 (± 0.02) yr + 0.099 (± 0.004) t – 0.0065 (± 0.0010) t^2 + 0.068 (± 0.017) *Chl a* + ε_3	0.13

829 The variables of yr is the year of sampling (yr_s) from 2013 ($yr = yr_s - 2013$), S is salinity, t is temperature (°C) from which 18.0 is subtracted,
830 and *Chl a* is the *Chl a* concentration (μg l^{-1}). The numbers in parentheses are standard errors. ε_1 to ε_3 is the residuals, and rms is root mean
831 square.

832